

ARTICLE

Electronic Supplementary Information

Cite this: DOI: 10.1039/x0xx00000x

Solid solubility of rare earth elements (Nd, Eu, Tb) in $In_{2-x}Sn_xO_3$ - effect on electrical conductivity and optical properties

Received 00th January 2012,
Accepted 00th January 2012

DOI: 10.1039/x0xx00000x

www.rsc.org/

Synthesis

Phase-pure and nano-crystalline powders of REE-doped In_2O_3 and ITO could successfully be prepared when tartaric acid (TA) and ethylene glycol (EG) were used as complexing agents. In initial investigations it was attempted to prepare REE-doped ITO powders with acetic acid (AA, CH_3COOH , p.a. Acros Organics) and EG as complexing agents, as this synthesis yielded phase-pure undoped ITO, as demonstrated in our previous work.¹ A brief review of the results from the initial syntheses is given here.

The syntheses with AA and EG resulted in amorphous gels, which indicated that no cation segregation occurred prior to gelation. However, after calcination at 600 °C for 3 h a relatively large fraction of the metastable rhombohedral In_2O_3 polymorph (space group $R\bar{3}c^2$) could be observed by XRD. The diffraction patterns of ITO with 1 and 5 cat% Nd prepared using these synthesis conditions are presented in Fig. S1. The phase contents of the syntheses with different dopants, doping concentration and calcination temperature are given in Table S1. The powders with 5 and 10 cat% REE generally had a significantly higher amount of the rhombohedral phase than the powders with only 1 cat% REE. The amount of the rhombohedral phase appears to be larger for Nd-doping, which has the largest size difference compared to In^{3+} of the three dopants. Increasing the calcination temperature from 400 to 600 °C slightly reduced the amount of the rhombohedral In_2O_3 polymorph.

In our previous work we demonstrated that the use of larger organic molecules as complexing agents promoted the formation of the stable cubic polymorph, at the expense of the metastable rhombohedral polymorph.¹ In order to prepare phase-pure powders of REE-doped ITO it was decided to try to replace AA with TA. When TA and EG were used as complexing agents phase-pure powders with the cubic In_2O_3 polymorph (space group $Ia\bar{3}$) were successfully obtained, as illustrated by the topmost diffractogram in Fig. S1.

The cubic bixbyite structure is the stable crystal structure for the RE_2O_3 compounds, as for In_2O_3 . Yet, unlike for In_2O_3 , the rhombohedral corundum structure is not even the stable

structure at high pressures for the RE_2O_3 compounds.^{3,4} It is not clear why the REE-doping increases the amount of the rhombohedral phase, but it is probably related to the kinetics of the crystallisation when the gel is decomposing to the final oxide materials.

Phase evolution of ITO:RE with increasing heat treatment temperature

XRD patterns of ITO:10%Eu after sintering at different temperatures are given in Fig. S2. No secondary phases could be observed at 600 and 800 °C. At 1000 °C and higher, secondary phases are present and it is evident that $EuInO_3$ (space group $P6_3cm^5$) forms at lower temperatures than the pyrochlore $Eu_2Sn_2O_7$ (space group $Fd\bar{3}m^6$). A similar phase evolution was observed for the ITO:10%Nd material. As In_2O_3 is the host, it is reasonable that it is easier for the RE-dopant to form a secondary phase with In^{3+} at lower temperatures where the cation mobility is limited, compared to the two co-dopants, RE^{3+} and Sn^{4+} forming the pyrochlore phase together.

Structural and microstructural properties of thin films

Thin films of selected compositions were successfully deposited by spin coating of the aqueous precursor solution. The prepared thin films appeared to be phase-pure and nano-crystalline by XRD, as evidenced by the four diffractograms of $In_2O_3:Eu$ given in Fig. S3. Also the other films had similar diffractograms to the ones given in Fig. S3. The cubic lattice parameters of the different films are given in Table S2 and the inset of Fig. S3. Spin-coated thin films deposited by the aqueous sol-gel process are subject to tensile strain which is only released by heat treatment at temperatures higher than 600 °C, which will have a large impact on the lattice parameter.⁷ The crystallite size in the thin films, calculated by the line broadening in XRD, was 14–16 nm and independent of the doping. The microstructures of selected thin films are displayed in Fig. S4. All of the films were continuous and homogeneous, with grain sizes of about 20 nm. The REE-doping did not seem to affect the microstructure or grain sizes, in line with the

crystallite sizes inferred from XRD. The thickness of the films is estimated to be about 100 nm based on our previous work.¹

Electrical properties and density

The electrical conductivity and thermopower of sintered materials of In_2O_3 and ITO doped with the REEs are given in Fig. 5 and in Table S2. The density of the sintered samples was shown to range between 58 and 92 %. The sintered density did not follow a clear trend regarding the REE doping concentration and relatively dense samples could be prepared from nano-crystalline powders with high concentrations of REEs (the density of In_2O_3 :10%Eu was 88 %). It has been known for decades that it is difficult to fabricate polycrystalline In_2O_3 and ITO with high density,⁸⁻¹⁰ also from nano-crystalline powders with a high driving force for densification.¹¹ In a previous sintering study of nano-crystalline In_2O_3 and ITO powders prepared by the same sol-gel synthesis, it was demonstrated that the degree of agglomeration in the nano-crystalline powders is a key property which has a significant effect on the obtained densities of the materials.¹¹ The degree of agglomeration could vary with composition, but can also differ between different prepared batches of the prepared nano-crystalline powders. It was attempted to remove hard agglomerates in the nano-crystalline powders by ball milling prior to the powder compaction, but the density was still low for some of the materials. Furthermore, the sintering temperature was not optimised for each composition despite that the sintering temperature is expected to vary significantly with doping level. Finally, the reported conductivities in Table S3 were corrected for porosity by the Bruggemann symmetric model,¹² and the differences in conductivity were so large, ranging over several orders of magnitude, which cannot be explained by variations in density.

Optical properties and band gaps

The transmittance of ITO:Eu thin films is given in Fig. S5, and the high transmittance of the TCO hosts was clearly not reduced by the presence of europium. Similar observations were made for In_2O_3 :Eu, both in transmittance and reflectance experiments. The absorption coefficient of the films was estimated based on the transmittance and reflectance, by the method developed by Cesaria et al.,¹³ and the band gaps were estimated by Tauc plots.¹⁴ The band gap is about 0.2 eV higher for ITO than for In_2O_3 due to the well-known Burstein-Moss effect.^{15,16} The band gap of the sintered materials was estimated from the diffuse reflectance spectra by the Kubelka-Munk method¹⁷ and is given in Fig. S6. The band gaps of the In_2O_3 -based materials appear to be slightly increasing with REE-doping, both for the thin films and the sintered materials. It is not straightforward to explain these results. The opposite trend was observed by Anand et al. where they claimed that the observed band gap narrowing was caused by Eu^{3+} forming new states in the band gap of In_2O_3 , which thereby serve as the new lowest occupied molecular orbitals.¹⁸ For the ITO-based films the band gap appears to decrease slightly with increasing amount of Eu-doping, which could be related to a smaller Burstein-Moss effect, compared to the pure ITO film. The difference in the absolute values of the estimated band gaps between the thin films and the sintered samples is related to the nature of the band gap of In_2O_3 . The band gap is around 2.9 eV and direct, but due to parity forbidden transitions electrons must be excited from energy bands about 0.8 eV below the

maximum of the valence band in order for strong transitions to occur.¹⁹ The weak transition will not occur in appreciable amounts in transmission spectroscopy of the thin films, but will dominate the response in the diffuse reflectance of the sintered pellets.

Luminescence decay measurements

Luminescence decay measurements were performed on nano-crystalline powders and sintered materials of In_2O_3 doped with 5 and 10 cat% Eu and the decay times are summarised in Table S3. The average lifetime of the material, accounting for the relative strength of the contributions from the different decays, are given as the weighted average. The decay of the nano-crystalline powders was fitted by three exponential decays, while two decays were used for the sintered samples. The lifetimes of sintered In_2O_3 doped with 5 and 10 cat% Eu were 0.867 and 0.782 ms, respectively. When only a single exponential was used for the sintered materials the corresponding lifetimes were 0.863 and 0.756 ms.

Acknowledgements

Financial support from NTNU is acknowledged.

Notes and references

- a Department of Materials Science and Engineering, Norwegian University of Science and Technology, N-7491 Trondheim, Norway. * E-mail: tor.grande@ntnu.no.
 b Department of Physics, Norwegian University of Science and Technology, N-7491 Trondheim, Norway.
 c Department of Materials Science and Engineering, Northwestern University, Evanston, IL 60208, USA.

- 1 T. O. L. Sunde, E. Garskaite, B. Otter, H. E. Fossheim, R. Saeterli, R. Holmestad, M. A. Einarsrud and T. Grande, *J. Mater. Chem.*, 2012, **22**, 15740.
- 2 A. N. Christensen, N. C. Broch, O. v. Heidenstam and Å. Nilsson, *Acta Chemica Scandinavica*, 1967, **21**, 1046.
- 3 G. Adachi and N. Imanaka, *Chem. Rev.*, 1998, **98**, 1479.
- 4 C. T. Prewitt, R. D. Shannon, D. B. Rogers and A. W. Sleight, *Inorg. Chem.*, 1969, **8**, 1985.
- 5 R. D. Shannon, *Inorg. Chem.*, 1967, **6**, 1474.
- 6 C. G. Whinfrey, D. W. Eckart and A. Tauber, *J. Am. Chem. Soc.*, 1960, **82**, 2695.
- 7 T. O. L. Sunde, M. A. Einarsrud and T. Grande, *submitted*,
- 8 M. J. H. W. De Wit, P. F. Elbers and M. Laheij, *Science of Ceramics*, 9, *Proc.*, 1977, **9**, 143.
- 9 T. Vojnovich and R. J. Bratton, *American Ceramic Society Bulletin*, 1975, **54**, 216.
- 10 N. Nadaud, M. Nanot and P. Boch, *J. Am. Ceram. Soc.*, 1994, **77**, 843.
- 11 T. O. L. Sunde, M. A. Einarsrud and T. Grande, *J. Eur. Ceram. Soc.*, 2013, **33**, 565.
- 12 D. S. McLachlan, M. Blaszkiewicz and R. E. Newnham, *J. Am. Ceram. Soc.*, 1990, **73**, 2187.
- 13 M. Cesaria, A. P. Caricato and M. Martino, *J. Opt.*, **14**, 10.

- 14 J. Tauc, Grigorov.R and A. Vancu, *Physica Status Solidi*, 1966, **15**, 627.
- 15 E. Burstein, *Physical Review*, 1954, **93**, 632.
- 16 I. Hamberg, C. G. Granqvist, K. F. Berggren, B. E. Sernelius and L. Engstrom, *Physical Review B*, 1984, **30**, 3240.
- 17 P. Kubelka and F. Munk, *Z. Tech. Phys.*, 1931, **12**, 593.
- 18 K. Anand, D. Singh, S. Kumar and R. Thangaraj, in *Preparation And Characterization Of Eu³⁺ Doped In₂O₃ Nanoparticles*, Amer Inst Physics, Melville, 2013.
- 19 A. Walsh, J. L. F. Da Silva, S. H. Wei, C. Korber, A. Klein, L. F. J. Piper, A. DeMasi, K. E. Smith, G. Panaccione, P. Torelli, D. J. Payne, A. Bourlange and R. G. Eggle, *Phys. Rev. Lett.*, 2008, **100**, 4.

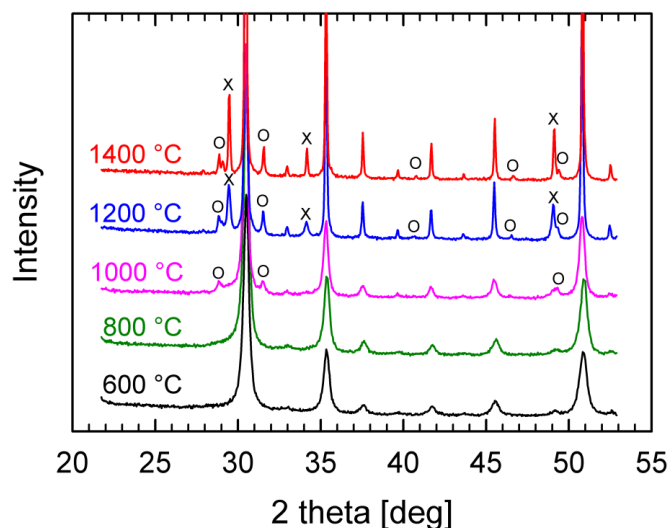


Fig. S2 XRD patterns of ITO:10%Eu after sintering at different temperatures. Diffraction lines from Eu₂Sn₂O₇ with space group $Fd\bar{3}m$ are marked by "X" and from EuInO₃ with space group P6₃cm by "O".

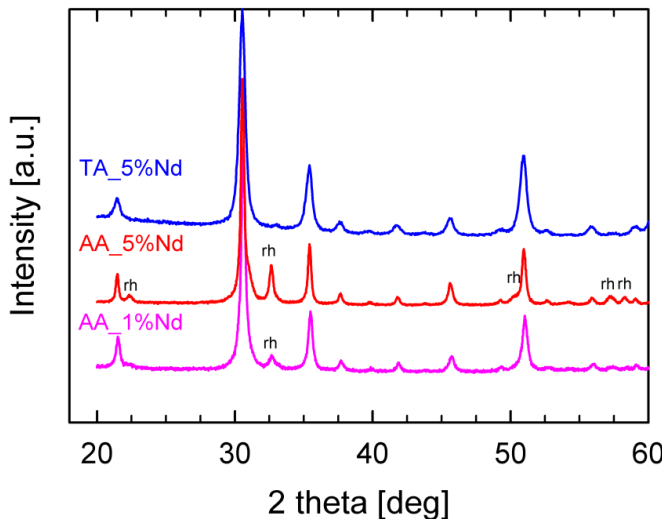


Fig. S1 XRD patterns of ITO powder doped with 1 and 5 cat% Nd after calcination at 600 °C. The two bottommost powders were prepared with acetic acid (AA) as a complexing agent, while in the topmost tartaric acid (TA) was used. Some of the strongest reflections from rhombohedral In₂O₃ (space group $R\bar{3}c$) are marked with "rh".

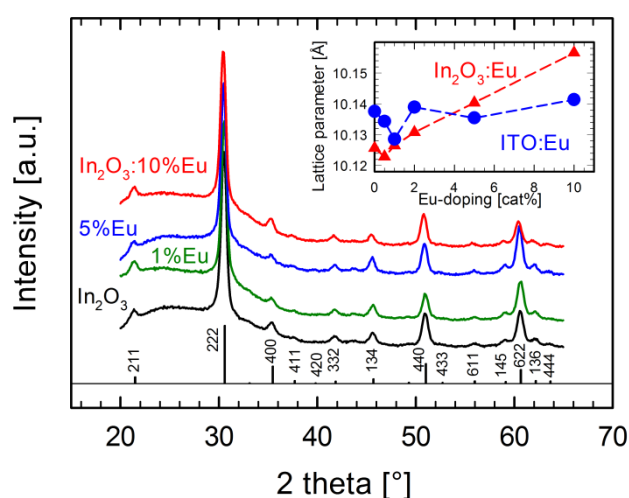


Fig. S3 XRD of In₂O₃ thin films with different amounts of Eu-doping. The reference pattern for the cubic In₂O₃ bixbyite structure with space group $Ia\bar{3}$ is given at the bottom. A broad bump centered at about 25 ° can be observed, which is caused by the amorphous glass substrate. Inset: Cubic lattice parameter for thin films of ITO:Eu (●) and In₂O₃:Eu (▲).

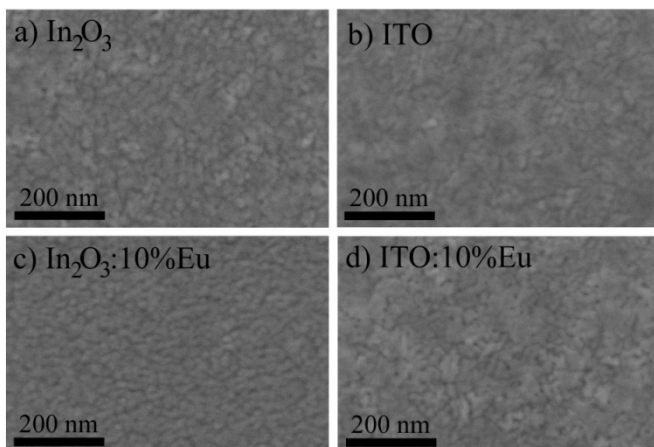


Fig. S4 SEM micrographs of the top surface view of thin films of In_2O_3 (a), ITO (b), $\text{In}_2\text{O}_3:10\%\text{Eu}$ (c) and ITO:10%Eu (d).

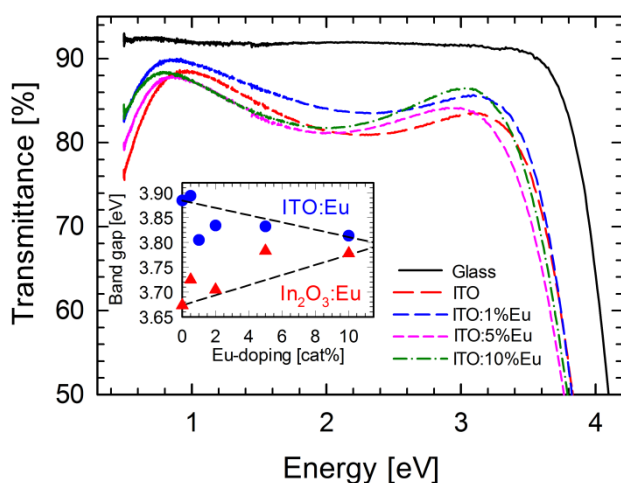


Fig. S5 Transmittance of selected ITO:Eu thin films on glass substrates. Inset: band gap of REE-doped In_2O_3 and ITO thin films. The dashed lines are guides to the eye.

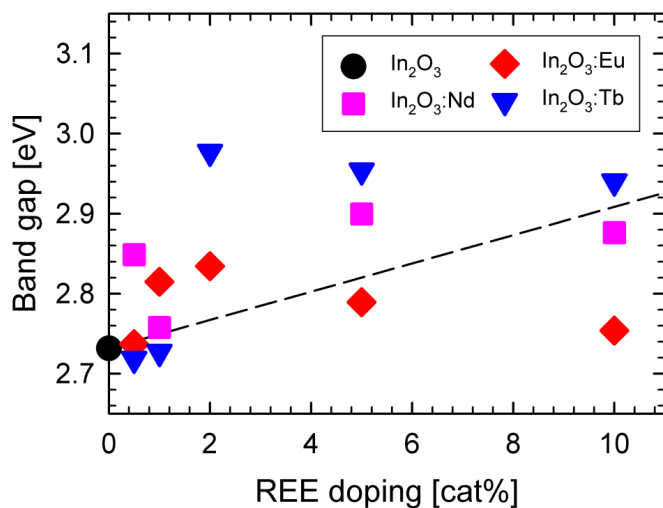


Fig. S6 Band gap of sintered materials of REE-doped In_2O_3 estimated from diffuse reflectance spectra using the Kubelka-Munk method. The dashed line is a guide to the eye.

ARTICLE

Table S3 Density, conductivity and thermopower of sintered materials of In_2O_3 and ITO doped with Nd, Eu and Tb. The estimated uncertainty is $\pm 2.5\%$ for the conductivity and thermopower and $\pm 0.2\%$ for the density.

Material	Doping amount [cat%]	Relative density [%]	Conductivity [S/cm]	Thermopower [$\mu\text{V/K}$]
ITO	0	92.3	$6.15 \cdot 10^3$	-30.4
ITO:Nd	1	90.4	$5.38 \cdot 10^3$	-30.0
ITO:Eu	1	85.4	$4.18 \cdot 10^3$	-30.5
ITO:Tb	1	86.2	$4.55 \cdot 10^3$	-31.3
In_2O_3	0	87.4	$1.31 \cdot 10^2$	-230
$\text{In}_2\text{O}_3:\text{Nd}$	0.5 1	59.1 74.9	$3.15 \cdot 10^0$ $1.99 \cdot 10^{-2}$	-222 -220
$\text{In}_2\text{O}_3:\text{Eu}$	0.5 1 2	82.0 64.6 59.4	$5.54 \cdot 10^1$ $1.76 \cdot 10^0$ $1.20 \cdot 10^{-1}$	-171 -249 -245
$\text{In}_2\text{O}_3:\text{Tb}$	0.5 1 2	84.3 85.5 58.5	$1.49 \cdot 10^2$ $4.89 \cdot 10^1$ $1.00 \cdot 10^1$	-197 -227 -235

Table S4 Decay times for emission at 611 nm after excitation for nano-crystalline powders and sintered materials of In_2O_3 doped with 5 and 10 cat% Eu after excitation at 530 nm. The value in parenthesis behind the decay times is the relative weight for each component of the fit.

Material	State	Heat treatment temperature [°C]	Decay [ms]	Weighted average [ms]
$\text{In}_2\text{O}_3:5\%\text{Eu}$	Nano-crystalline powder	530	$\tau_1 = 0.20 \pm 0.01$ (53.0 %) $\tau_2 = 0.67 \pm 0.01$ (35.5 %) $\tau_3 = 0.041 \pm 0.002$ (11.7 %)	0.35
$\text{In}_2\text{O}_3:10\%\text{Eu}$	Nano-crystalline powder	530	$\tau_1 = 0.18 \pm 0.02$ (49.5 %) $\tau_2 = 0.62 \pm 0.02$ (30.9 %) $\tau_3 = 0.042 \pm 0.001$ (19.6 %)	0.29
$\text{In}_2\text{O}_3:5\%\text{Eu}$	Sintered material	1400	$\tau_1 = 0.84 \pm 0.01$ (92.7 %) $\tau_2 = 1.19 \pm 0.03$ (7.3 %)	0.87
$\text{In}_2\text{O}_3:10\%\text{Eu}$	Sintered material	1400	$\tau_1 = 0.24 \pm 0.01$ (8.7 %) $\tau_2 = 0.83 \pm 0.01$ (91.3 %)	0.78